RSC Advances




ROYAL SOCIETY OF CHEMISTRY

www.rsc.org/advances

# GRAPHENE-BASED STRUCTURAL ADHESIVE TO ENHANCE ADHESION PERFORMANCE

Liberata Guadagno[1,2 *], Maria Sarno[1,2], Umberto Vietri[1], Marialuigia Raimondo[1], Claudia Cirillo[1,2], Paolo Ciambelli[1,2]

[1]*Department of Industrial Engineering – DIIn - University of Salerno*
*Via Giovanni Paolo II,132 - 84084 Fisciano (SA), Italy (UE)*

[2]*Centre NANO_MATES – University of Salerno*
*Via Giovanni Paolo II,132 - 84084 Fisciano (SA), Italy (UE)*

***Corresponding author: e-mail: lguadagno@unisa.it***

**Abstract**

This paper proposes the design of a new graphene nano-modified formulation to enhance the mechanical performance of structural adhesives. Well characterized graphene platelets, produced through an effective approach for bulk production and morphology control, were embedded at different content inside an epoxy adhesive based on tetraglycidylmethylene dianiline (TGMDA). The adhesive formulations were used to manufacture bonded joints, according to the ASTM 2095, in order to analyze the effect of graphene platelets on the tensile strength of the joints. The effect of incorporating graphene in the adherents was also considered. Epoxy adhesives filled with graphene at concentration up to 1%wt significantly enhanced the mechanical behavior of the bonded joints. Only in the case of unfilled adherents, the inclusion of 4%wt graphene has not a significant effect on the mechanical performance. This is likely due to nanofiller agglomerations causing heterogeneity in large domains at the interface between adherents and adhesive. The effect of graphene incorporation in the adherents, acting on the chemical compatibility between adhesive and adherent surfaces, led to a considerable increase of tensile strength in comparison with the corresponding joints with unfilled adherents. This beneficial effect is very likely due to cumulative effects of intermolecular interactions between graphene platelets and resin network.

**Keywords:** Thermosetting polymers, Adhesion of polymers on surfaces, Graphene**,** Mechanical properties of nanoscale systems, Nanotechnology nanoscale materials and structure

## 1. Introduction

Adhesively bonded joints are increasing alternatives to mechanical joints in engineering applications and provide many advantages over conventional mechanical seal. Adhesive bonding gives structural design possibilities which cannot be obtained by any other technique. Furthermore, in most load cases (tension, compression, shear) adhesive bonded structures are characterized by lower weight. Bonded joints are gas and moisture tight (unlike riveted or bolted joints) with good durability, excellent resistance against corrosion and good fatigue properties. Currently, structural bonding is still not a widely accepted alternative to riveting. However, if some disadvantages are overcome, the advantages of adhesive bonding make up for the disadvantages. The current challenge is therefore to overcome drawbacks such as the electrical insulating properties, water sorption and then debonding, flammability and critical points related to the processing temperature. In this paper, a formulation designed for structural adhesive to enhance mechanical performance of epoxy adhesives nano-modified by graphene is shown. Graphene platelets were embedded inside an epoxy adhesive based on a mixture of tetraglycidylmethylene dianiline (TGMDA) and 1,4-butanedioldiglycidylether (BDE). This particular epoxy formulation has proven to be very effective for improving nanofiller dispersion due to a decrease in the viscosity [1-2], and, in addition, it was found that it allows to reduce the moisture content which is a very critical point for adhesive bonding. The chemical composition of this epoxy formulation reduces the equilibrium sorption of liquid water ($C_{eq}$) of about 35% [3-4]. This is a very large value in the application of epoxy mixtures as structural adhesive materials; for example, in the aeronautics, absorbed moisture reduces the matrix-dominated mechanical properties. Absorbed moisture also causes the adhesive to swell, and during freeze-thaw cycles expands during freezing and can crack the material. The particular epoxy matrix also proved to be beneficial for improving the cure degree. It increases the mobility of the chains containing the reactive groups resulting in a higher cure degree than the epoxy precursor alone [4].

Several papers have been published on the inclusion of nano-structured carbon forms, including graphene, inside epoxy adhesives in order to enhance the mechanical strength and toughness of the bonded joints [5-9]. At the same time, it is well known in literature that one of the main predicted advantages related to the inclusion of conductive nanoparticles into epoxy resin is the improvement of its electrical behavior [10-16]. Different types of carbon nanofillers are electrical conductor materials, which, if well dispersed in the matrix, can drastically increase the electrical properties of epoxy based adhesives also at very low percentage of nanofiller, and especially graphene exhibit fascinating physical properties such as thermodynamic stability, extremely high charge carrier mobility and mechanical stiffness, critical requisites for several applications [17-23]. Recently, Bunch et al. have highlighted another relevant feature of graphene sheets; atomic membranes from graphene sheets are impermeable to standard gases including helium and can support pressure differences larger than one atmosphere [24]. We would expect a similar performance for bulk polymer containing homogenously dispersed graphene sheets. This outstanding feature is of potential interest in the field of structural adhesives. Moreover, graphene based materials can activate self-assembling mechanisms able to improve gas barrier and mechanical properties of nanocomposites [25-26].

The enhancement of different properties of epoxy-based materials and or/adhesives depends of numerous parameters, such as the chemical nature of nanofiller, adhesive and adherents, the applied surface treatment or the tested properties [16]. Concerning the chemical nature of the nanofiller, the structure and the different morphological parameters, strongly dependent on the preparation procedure, may vary in a wide range of values so as to determine very different effects on the adhesive performance. For this reason, graphene well characterized and prepared using an approach for bulk production and morphology control, has been used in this work.

Since the first successful fabrication of graphene by cleavage, three major methods for the fabrication of single-and multi-layer graphene have been investigated. These methods include micromechanical cleavage [17], exfoliation of graphite [27-28] and chemical vapor deposition

(CVD) of hydrocarbons on a substrate surface [20, 29–33]. Among them, exfoliation of graphite results to be the much more efficient approach for bulk production of graphene platelets.

Moreover, several papers concern the exfoliation of graphene oxide (GO) [19, 34–35]. This material consists of graphene-like platelets, chemically functionalized with compounds such as hydroxyls and epoxides, which stabilize the platelets in water [27]. However, GO has poor quality and the required reduction often results in the generation of a significant number of defects [27, 34]. On the other hand, defect free, unoxidized graphene can be obtained by a non-covalent, solution-phase method [28]. Hernandez et al. obtained high-quality monolayer graphene at significant yields (1 wt%) via non-chemical, solution-phase exfoliation by sonicating graphite in organic solvent. Graphene used for this work was prepared by liquid phase exfoliation in N-methylpyrrolidone (NMP). The sonication parameters have been modulated to treat an elevated graphite concentration solution to obtain an high graphene yield and an one step massive production of thin platelets .

The incorporation of graphene platelets, prepared using the above procedure, on the adhesive performance was studied. A suitable fraction of graphene platelets inside the epoxy paste leads to an enhancement of joint strength. Epoxy matrix nanofilled up to 1wt% significantly enhanced the mechanical behavior of the bonded joints, whereas the addition of 4wt% graphene has a non beneficial effect on the adhesive performance, probably due to nanofiller agglomerations responsible for the destruction in the continuity of the morphological features of the adhesive. The incorporation of graphene platelets in the adherents led to a considerable increment of tensile strength in comparison with the corresponding joints with unfilled adherents.

## 2. Experimental section

### 2.1. Materials

*Epoxy matrix.* The epoxy matrix was prepared by mixing the epoxy precursor TGMDA (Epoxy equivalent weight 117-133 g/eq), with an epoxy reactive monomer 1,4-

butanedioldiglycidylether (BDE) that acts as reactive diluent. These resins, both containing an epoxy, were obtained by Sigma-Aldrich. The curing agent investigated for this study is 4,4'-diaminodiphenyl sulfone (DDS). The hardener was used at stoichiometric concentration with respect to oxirane rings. In this paper, the epoxy mixture is labeled as T20BD.

*Nanofiller.* Graphite powder was purchased from Alfa Aesar (microcrystalline, -300 mesh). N-methylpyrrolidone was purchased from Sigma Aldrich (spectrophotometric grade> 99.0%).

### 2.2. Sample preparation

*Graphene.* Graphene platelets were prepared by liquid phase exfoliation of graphite. The graphite was dispersed in N-methylpyrrolidone (NMP) at a concentration of 10 mg/ml and sonicated for 1 h. This method allows to produce high-quality, unoxidized graphite and graphene platelets from powdered graphite. In this way, colloidal dispersions of graphene platelets are obtained through the exfoliation of graphite in the liquid phase in suitable organic solvents. This is possible because the energy required to exfoliate graphene is balanced by the solvent–graphene interaction, for solvents whose surface energies match that of graphene. Different techniques were used to demonstrate the presence of individual graphene and the distribution of the platelets thickness (i.e by transmission electron microscopy and electron diffraction, Raman spectroscopy, thermogravimetric analysis).

The best result, obtained dispersing graphite in N-methylpyrrolidone (NMP, spectrophotometric grade> 99.0%) (cylindrical vial, 10-25 ml solvent) at a concentration of 10 mg/ml for 1 h at the maximum power of ultrasound (Hielscher UP 400S), is reported in the following. The product of sonication was a liquid consisting of a greyish homogeneous phase and containing a number of macroscopic aggregates that can be removed by centrifugation for 90 minutes at 500 rpm.

Graphene and multilayer graphene platelets (G+MLG) were recovered by vacuum filtration of the supernatant solution from centrifugation onto 20 nm pore size alumina membrane. The supernatant contains about 30 wt% of the original graphite (see TG evaluation under Results and discussion section).

*Adherents and adhesive.* In this study, 0.5%, 1% and 4 wt/wt % of graphene was dispersed in epoxy resin to obtain an adhesive formulation to bond unfilled and filled epoxy adherents. Epoxy blend and DDS were mixed at 120°C and the graphene platelets were added and incorporated into the matrix by using ultrasonication for 20 min. An ultrasonic device, Hielschermodel UP200S (200 W, 24 kHz) was used. The combinations are shown in Table 1.

**Table 1** Summary of the prepared samples

| **Sample label** | **Adherent** | **Adhesive** | **Adhesive thickness [mm]** tensile butt joint |
|---|---|---|---|
| A | T20BD | T20BD | 0.19 ± 0.15 |
| B | T20BD | T20BD /0.5% wt/wt Graphene | 0.2 ± 0.05 |
| C | T20BD | T20BD / 1% wt/wt Graphene | 0.15 ± 0.1 |
| D | T20BD | T20BD / 4% wt/wt Graphene | 0.18 ± 0.05 |
| E | T20BD /0.5% wt/wt Graphene | T20BD /0.5% wt/wt Graphene | 0.15 ± 0.05 |
| F | T20BD /1% wt/wt Graphene | T20BD /1% wt/wt Graphene | 0.18 ± 0.05 |
| G | T20BD /4% wt/wt Graphene | T20BD /4% wt/wt Graphene | 0.15± 0.15 |

Adhesive formulations were cured by a two stage curing cycle: an initial step at moderate temperature (125°C for 1 h) and the second one at higher temperature (180°C for 3 h).

### 2.3. Characterization techniques

Field Emission Scanning Electron Microscopy (FESEM) images were captured with a LEO 1525 microscope. Transmission Electron Microscopy (TEM) images were acquired with a FEI Tecnai electron microscope operating at 200 kV with a $LaB_6$ filament as source of electrons. The samples for the TEM observation were casted from NMP solution on the TEM grid.

Raman spectra of both the supernatant and precipitate from centrifugation, casting on a glass slip and after NMP drying, were obtained at room temperature with a microRaman spectrometer (Renishaw inVia; 514 nm excitation wavelength). For the all the samples about 100 measurements have been carried out. The laser spot diameter was 10 μm, a value higher than the size of the obtained platelets.

X-Ray Diffraction (XRD) measurements were performed with a Bruker D8 X-ray diffractometer using CuKα radiation. The measurements were performed on the thin carbon film obtained after filtration.

The thermal decomposition behaviour was investigated with a thermo-analyzer (Q600, TA Instruments) online connected to a quadrupole mass detector (Quadstar 422, Pfeiffer Vacuum). The measurement was carried out in air flow.

Adhesive performance of nanofilled epoxy-based materials was investigated considering bonded joint configurations which refer to ASTM D2095 standard.

Materials (unfilled and filled epoxy mixture) were cured in an appropriate mold geometry configuration made of teflon (PTFE). The mold was designed following the existing international standard practice in the design of the specimens; in particular, ASTM D 2094 and ASTM D 1002 were considered. In this way a suitable configuration of specimens for tensile butt joint (referred to ASTM D 2095), was respectively obtained to measure mechanical strength and hence adhesion properties of bonded joint (see scheme 1).

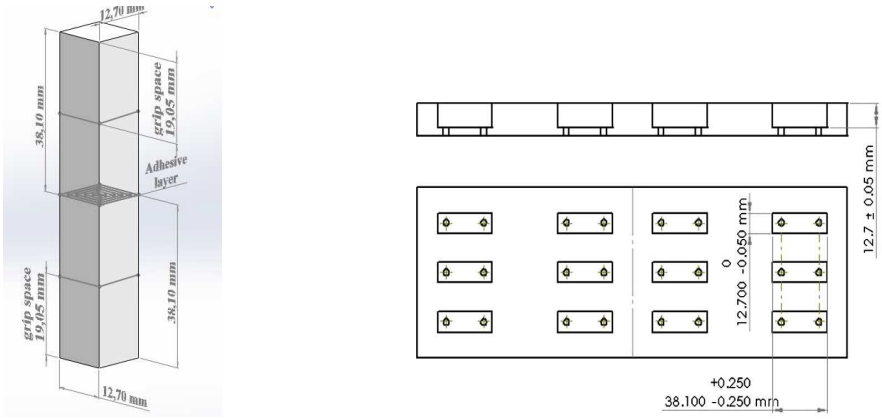


**Scheme. 1 (a)** Schematic of the tensile butt joint strength test specimens (referred to ASTM D 2095), (b) Schematic of the mold (referred to ASTM D 2095).

FESEM investigation was carried out using FESEM (FE-SEM, mod. LEO 1525, Carl Zeiss SMT AG, Oberkochen, Germany) with the aim of studying the morphology of the detached zones. The fracture surfaces of the bonding areas were preliminary coated with a thin gold layer of 250 Å.

*Mechanical testing.* Adhesive tests were carried out using an electro-hydraulic servo-controlled testing machine (Instron mod. 4301). Tensile strength of the nano-reinforced interface were measured. The loading was applied according to ASTM D 2095 standard requirement. In tensile butt joint tests, 20 MPa/cm$^2$ of bond area per min (3.1 kN/min) was applied; a load cell of 5kN needed for this aim. This arrangement also ensures that no slip would take during the test. Five samples were prepared for each set, as required by ASTM D 2095, and average values of the mechanical strength of the joints were measured. For this purpose, the maximum tensile load measured during the tests was divided by transversal bonded area. The elastic modulus of adhesive paste was determined by tensile test on bulk specimens (ASTM D 638 standard requirements). Several samples were tested for each set in tensile mode by applying a loading rate of 1 mm/min. In any case, the Young's modulus was calculated as the slope of the stress-strain curve in the linear region.

## 3. Results and discussion

### 3.1. Graphene characterization

FESEM images at increasing magnification of the obtained platelets are shown in Fig. 1, the powder consists of platelets of nanometric size.

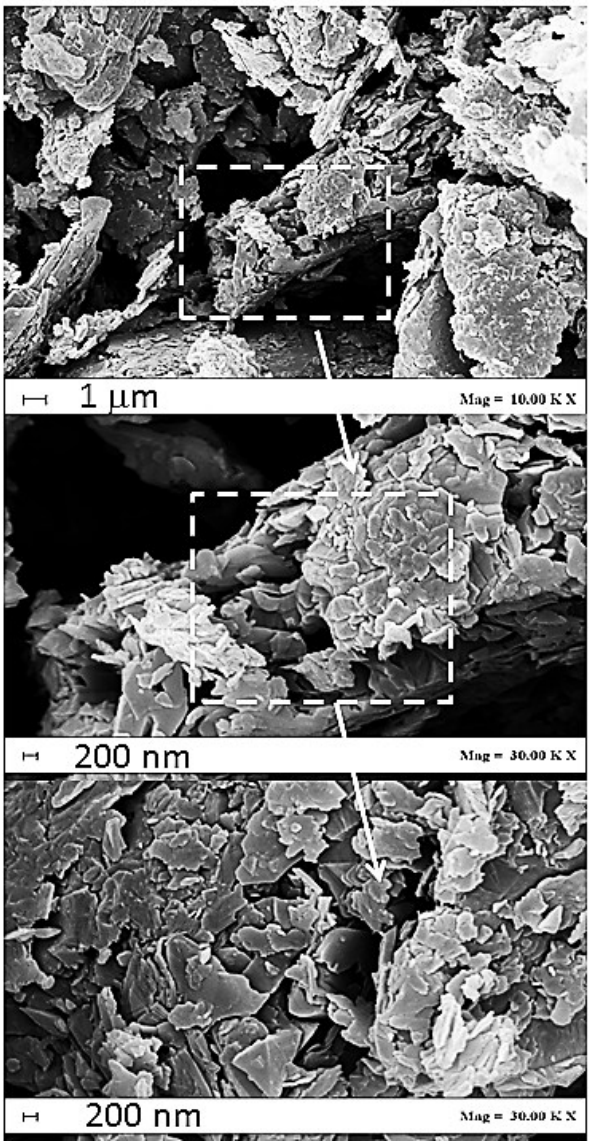


**Fig. 1** FESEM images of the platelets of graphene and multilayer graphene platelets, at increasing magnification.

To investigate the state of the material remaining dispersed in the supernatant solution after the centrifugation, TEM images have been obtained by dropping a small amount of the dispersion onto holey carbon grids. Fig. 2 shows two typical bright-field TEM images, at two different magnifications.

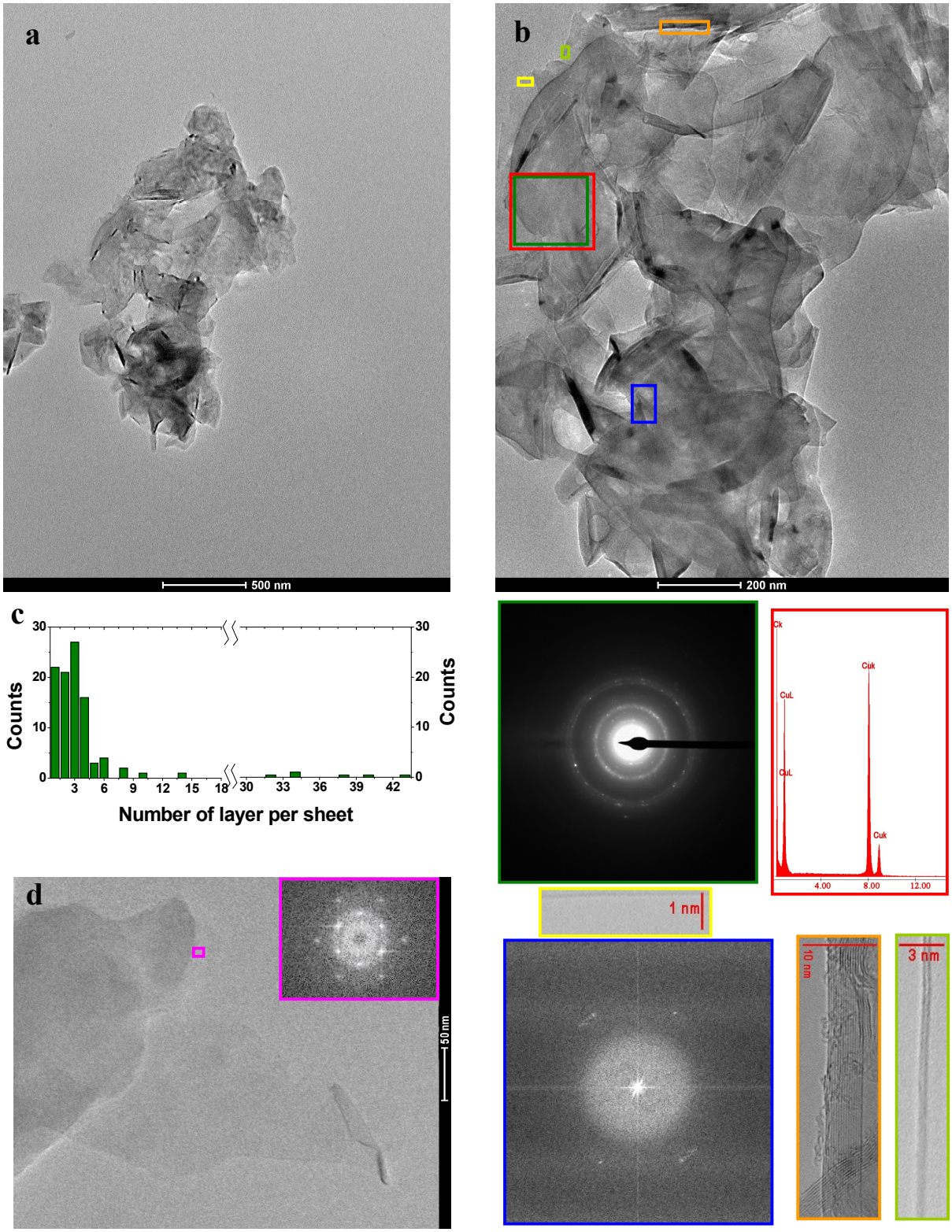


**Fig. 2** TEM images at two different magnifications of the platelets of graphene and multilayer graphene platelets (a, b). The inserts in Figure 2b are: electron diffraction pattern, in the green area; EDAX analysis, in the red area; FFT in blue area; high resolution TEM images, in orange, light green and yellow areas. Histogram of the number of layer per platelet (c). Higher resolution TEM image and electron diffraction pattern collected in the pink area (d).

The TEM images of all samples reveal the presence of platelets of graphene and multilayer graphene platelets, having lateral sizes typically of a few micrometers. In many cases the platelet edges tend to scroll and fold slightly. The corresponding electron diffraction pattern (insert in the green area) and the EDX spectrum (insert in red area) confirm the carbon $sp^2$ nature of the platelets. The FFT recorded in the area in blue evidences different orientations of packed multilayer with the typical interlayer graphite spacing of about 0.34 nm. The high resolution TEM images in the inserts of Fig. 2b permit to count the number of layers of the platelets whose edges are in the areas highlighted by colored rectangles: 15 and 12, 2 and 1 in orange, in light green and in yellow, respectively.

By statistic analysis of over 200 objects in the large number of TEM images, we generated an histogram of the platelets thickness statistics as shown in Fig. 2c (normalized on 100 objects). From these data the percentage of monolayer graphene in NMP dispersions can be estimated. We found that the ratio number of monolayers/total number of platelets was 0.22, corresponding to a monolayer mass fraction (mass of monolayers/mass of all platelets) of 0.055, leading to an overall yield of 1.65 wt. % (the supernatant contains about the 30 wt% of the original graphite, TG evaluated see in the following).

In Fig. 2d an higher resolution TEM image and the electron diffraction pattern, collected in the pink area of the figure, are also reported. The electron diffraction pattern exhibits the typical sixfold symmetry expected for graphite/graphene [36], permitting the definitive identification of graphene in the area in pink.

In particular, a TEM image, showing a number of platelets including monolayer, is reported in Fig. 3a, together with the electron diffraction patterns obtained in the orange and green area, respectively. Labelling the two sixfold symmetry with the Miller–Bravais (hkil) indices and considering that for the multilayers, the (2110) spots appear to be more intense relative to the (1100) spots (computational studies have shown that the intensity ratio for multilayer, with Bernal (AB) stacking, is $I_{(1100)}/I_{(2110)}<1$, whereas for monolayers it is $I_{(1100)}/I_{(2110)}>1$ [28]) we identify graphene in the

orange area and multilayer graphene in the green area. Starting form this considerations, we obtain the histogram reported in Fig. 3e by measuring the diffraction pattern of 100 thin platelets and the relative intensity ratio $I_{(1100)}/I_{(2110)}$, finding that on the respect of the more thinner platelets, the monolayer fraction is about 0.4.

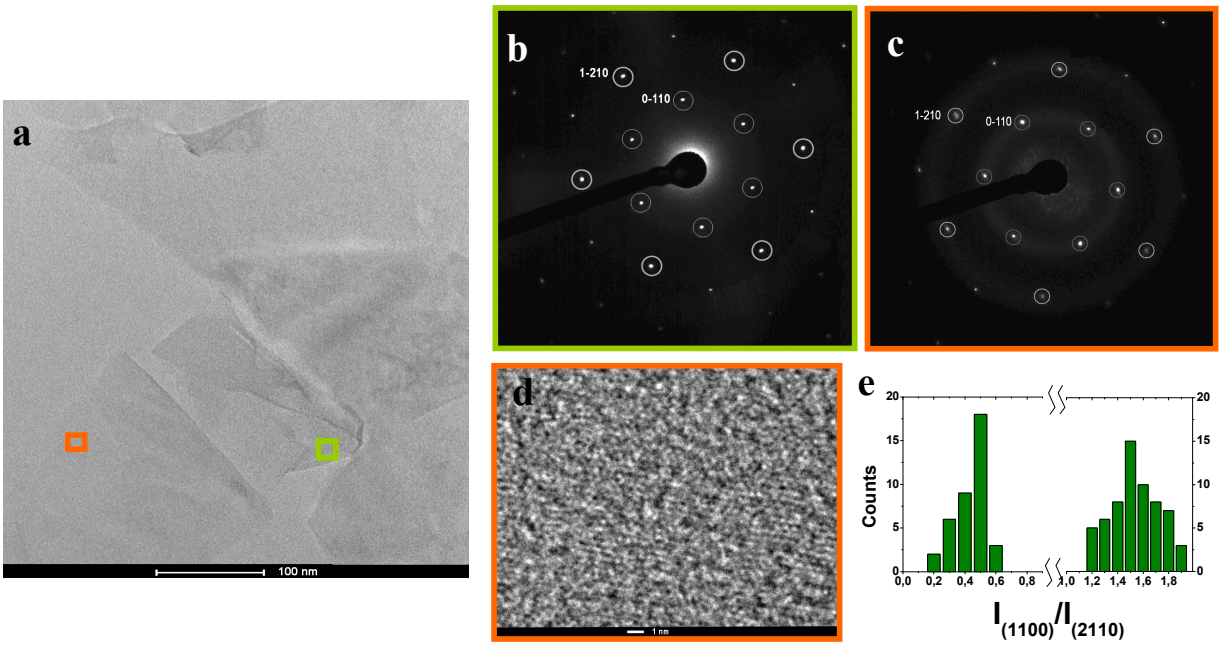


**Fig. 3** TEM image of the graphene and multilayer graphene (a); electron diffraction pattern of multilayers in the green are (b); electron diffraction pattern and high resolution TEM image of a monolayer in the orange area (c,d). Histogram of the intensity ratio $I_{(1100)}/I_{(2110)}$ obtained on 100 thin platelets (c).

The XRD diffraction patterns of graphite and G+MLG, are reported in Fig. 4.

The characteristic reflection (002) of the samples can be compared in order to understand the structural changes before and after the exfoliation. The peak intensity of pristine graphite results higher than that of G+MLG indicating graphite delamination into more thinner graphene and multilayer graphene platelets [37]. The lower downshift of the (002) reflection (from 27.0° to 26.7°) indicates a slightly higher interlayer distance (from 3.0 to 3.3 nm) between the graphene layers in the platelets after graphite exfoliation.

Fig. 5a shows two typical Raman spectra collected on the precipitate obtained after centrifugation and drying, are reported.

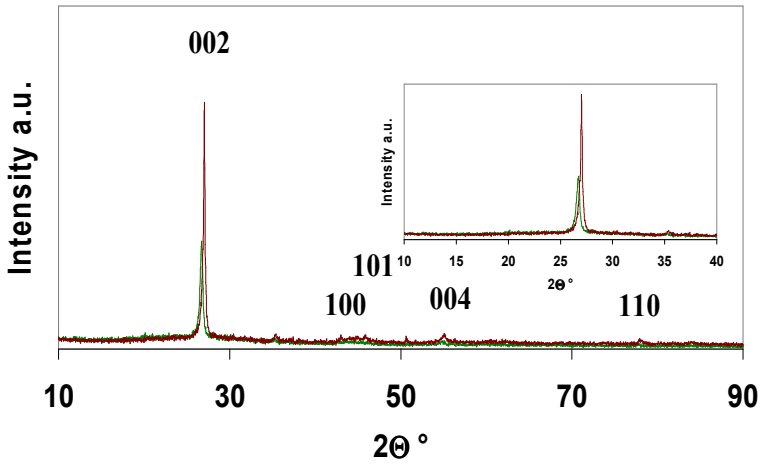


**Fig. 4** X-ray diffraction pattern of the platelets of graphene and multilayer graphene platelets, as recorded on the thin film obtained after vacuum filtration.

The two most intense features are the G peak at ~1570 $cm^{-1}$ and a band at ~2700 $cm^{-1}$, named 2D, since it is the second most prominent peak always observed in graphite samples [38]. The G peak is due to the doubly degenerate zone center E2g mode [39], while the 2D band is the second order of zone-boundary phonons. Such phonons give rise to a peak at about 1350 $cm^{-1}$ due to disorder or edge in graphite, called D band [39]. The G band for both the spectrum of Fig. 5a is centered at 1565 $cm^{-1}$. The 2D band in one case (profile in brown) is the typical of graphite consisting of the two components 2D1 and 2D2, the second with an highest intensity than the first [36]; the profile in orange have the same brown width, a flat apex and can be easily deconvolved with almost two peaks. A broad D-band can be seen in both the spectrum collected in Fig. 5a, in [28] has been demonstrated that this exfoliation process does not introduce significant structural defect, on the other hand our laser spot diameter was 10 μm, a value higher than the size of the obtained platelets suggesting the presence of edges within the analyzed area. Additionally, the so-called G* band [40] can be seen at 2450 $cm^{-1}$.

Spectra in Fig. 5b were measured on thin films of G+MLG prepared by vacuum filtration of the supernatant onto alumina. Fig. 5b shows a significant change in shape and intensity of the spectra

collected from the supernatant compared to precipitate. An up shift of about 7 $cm^{-1}$ of the G band and a downshift of the 2D band, typical of thinner graphite platelets, are observed [41].

Considering the laser spot size and the platelets dimensions, a certain number of platelets were contemporaneously tested. The Raman Spectra collected are, thus, the results of the vibration contributions of different platelets. The spectra collected in the fig. 5 are two of the most typical. More than 100 spectra have been collected for the two samples, finding very little differences. What we intend to highlight is the difference between the two phases obtained by graphite exfoliation

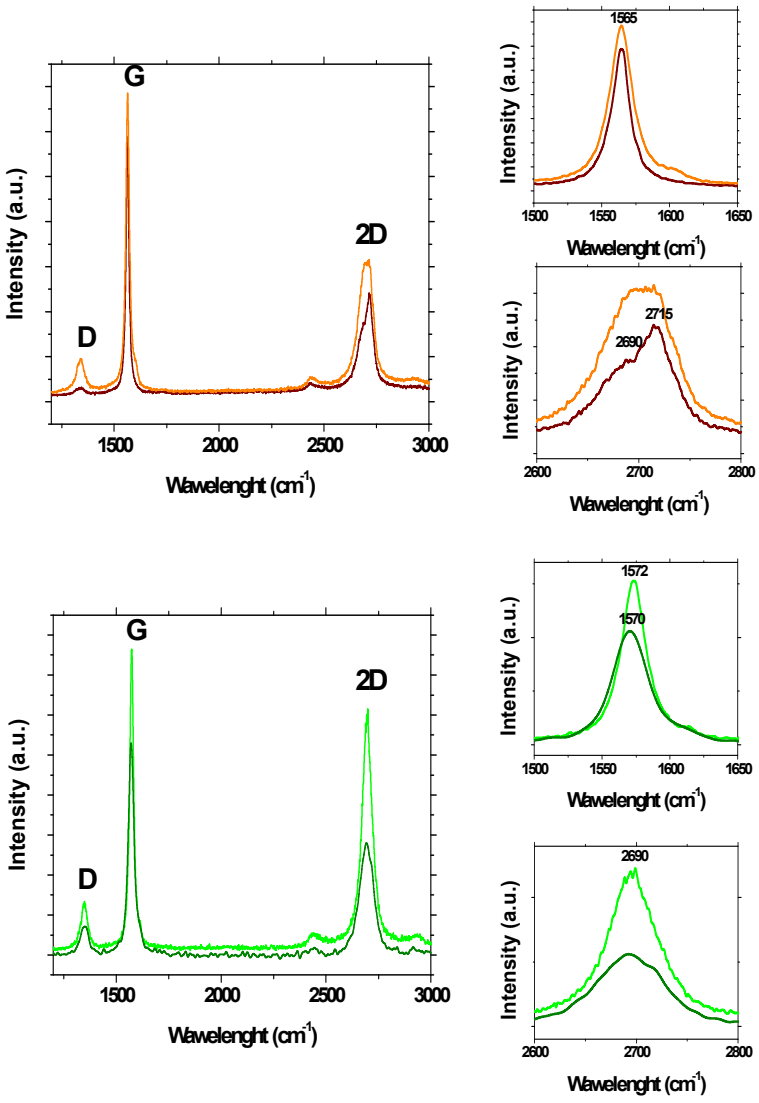


**Fig. 5** Raman spectra of the: centrifugation precipitate (a) and of the platelets of graphene and multilayer graphene obtained after centrifugation (b).

The oxidation process of pristine graphite and G+MLG after drying was compared by thermal analysis (Fig. 6a). The oxidation occurred as a weight loss step in the temperature range 530–875°C, with a DTG peak centered at 702°C for graphite, that results slightly downshifted to 695°C for the obtained sample. The TG residue of the graphite is likely due to its original purity degree. For both samples the oxidation step is characterized by $CO_2$ release (see m/z=44), while no fragments from NMP or other impurities can be seen during the thermogravimetric test, indicating the high degree of purity of the obtained sample, for which in addition the thermogravimetric residue is practically zero.

In Fig. 6b the thermal conversion of NMP is reported, showing a weight loss in the range 25-150°C, the decomposition of the solvent is clearly indicated by the corresponding TIC of the most intense mass fragment peaks (m/z=15, 18, 27, 28, 30, 39, 41, 42, 44, 56, 71, 72, 98, 99). The detector of the spectrometer continues to see the typical fragments of NMP, even after the oxidation event was finished, probably due to the high saturation level of the oxidation chamber.

The thermogravimetric profiles of the precipitate before drying is finally reported in Fig. 6c. It has been used to evaluate the amount of graphitic carbon in the precipitate, previously opportunely weighted, for quantitative evaluation. The TG profile shows two weight loss: the first one, in the temperature range 25-175°C, due to NMP as confirmed by corresponding TIC of the most intense mass fragment peaks also shown in the figure; the second one due to the graphite content. NMP constitute the 75 wt% of the precipitate. The increased end set temperature observed probably due to the interaction between the graphite layers and the solvent.

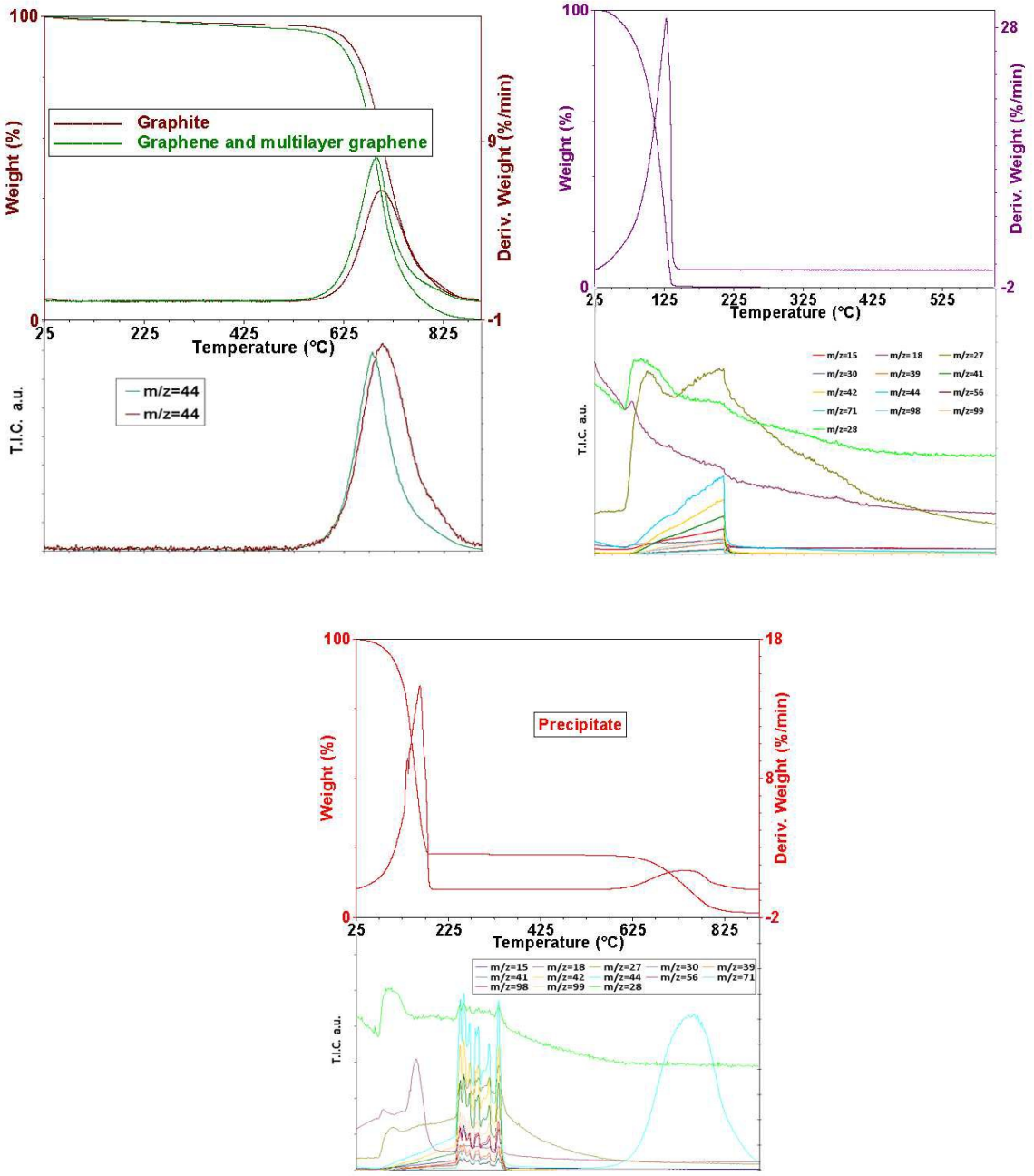


**Fig. 6** TG-DTG and relevant total ion current signals of graphite and G+MLG. TG-DTG and relevant total ion current signals of NMP. TG-DTG and relevant total ion current signals of the precipitate.

### 3.2. Mechanical characterization of adhesive paste

The tensile strength average values of different bonded joint are listed in Table 2 with the respective standard deviations. In this table, the composition of adherents and adhesive is shown once again to facilitate the text comprehension.

**Table 2** Summary of Tensile strength values for all sets of composite specimens

| Sample label | Adherent | Adhesive | Tensile Strength [MPa] |
|---|---|---|---|
| A | T20BD | T20BD | 9.090 ± 1.650 |
| B | T20BD | T20BD /0.5% wt/wt Graphene | 12.74 ± 4.272 |
| C | T20BD | T20BD /1% wt/wt Graphene | 18.06 ± 1.717 |
| D | T20BD | T20BD /4% wt/wt Graphene | 10.74 ± 0.217 |
| E | T20BD /0.5% wt/wt Graphene | T20BD /0.5% wt/wt Graphene | 16.98 ± 0.113 |
| F | T20BD /1% wt/wt Graphene | T20BD /1% wt/wt Graphene | 18.20 ± 1.864 |
| G | T20BD /4% wt/wt Graphene | T20BD /4% wt/wt Graphene | 16.47 ± 0.131 |

Stress–strain curves are displayed in Fig. 7.

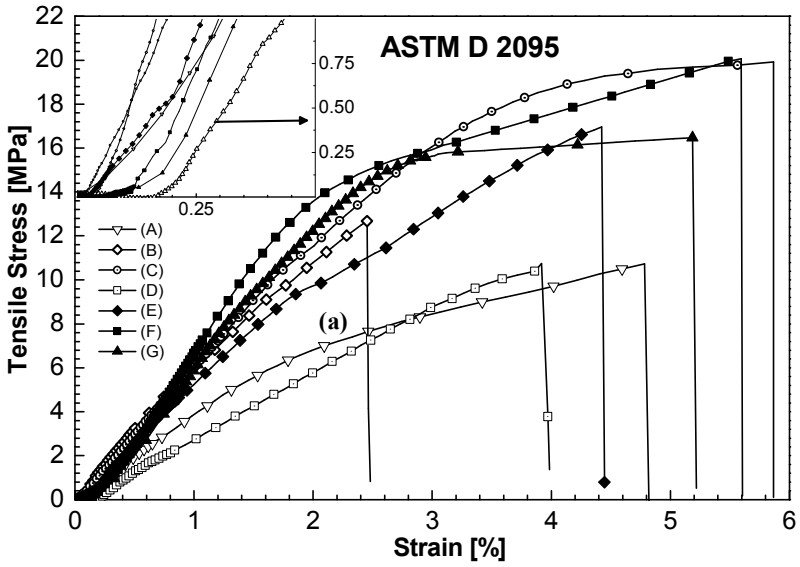


**Fig. 7** Stress-strain plot of bonded joints in Tensile tests ASTM D 2095.

Data in Table 2 highlight that the inclusion of graphene in the adhesive paste up to 1% wt/wt significantly enhances the joint strength (see samples B and C with respect to sample A), leading to

a significant improvement in mechanical behavior of the bonded joint. Nevertheless, for sample D, which corresponds to the highest concentration tested (i.e. 4 wt/wt % ), the improvement in the tensile strength value is much lower with respect to the samples B and C. It is very likely that this behavior is due to a poor nanofiller dispersion in the adhesive formulation caused by aggregations of the nanofiller as confirmed by morphological analysis of the fracture surface of the bonding areas of sample D (the morphology of this last sample will be discussed later on and illustrated in Fig. 11). The incorporation of graphene also into the adherents leads to a considerable increase of tensile strength for the samples E and G in comparison with the corresponding B and D samples containing unfilled adherents. The comparison of sample C with sample F, which contains 1% wt/wt % of graphene also in the adherent, highlights that sample F manifests the best performance in tensile test. In fact, even if only a very slight increase with respect to the corresponding sample C with unfilled adherents is detected, it is important to highlight that for this sample, replicated tests indicate that the failure mode of the joint occurs in the adherents as shown in Fig. 8. Therefore, for this sample, tensile strength of the bonded area might be potentially higher than the value shown in table. A comprehensive analysis of the results suggests that the incorporation of graphene in the adherents seems to reduce the gap in tensile performance between the samples at different graphene percentages. Furthermore, the higher values detected in tensile strength of samples E, F and G with respect to B, C and D highlight that, in the case of joints containing graphene platelets embedded in the adherents, the failure between adhesive and adherents is more hampered than the joints with unfilled adherents. This is a clear indication that graphene platelets at the interfaces between adhesive past and adherents act in such a way to strengthen the attractive intermolecular forces.

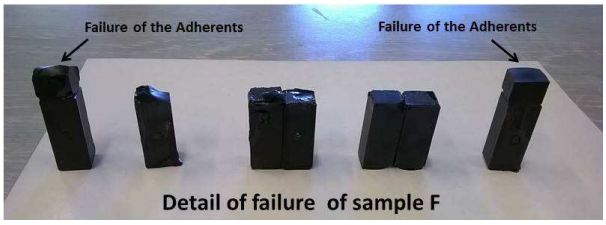


**Fig. 8** Detail of failure in sample F.

Young's modulus measured on bulk specimens are reported in Table 3. It slightly increases with increasing graphene concentration.

**Table 3** Young's modulus measured on bulk specimens

| Sample Label | Young's Modulus [MPa] |
|---|---|
| T20BD | 2087.5 ± 15.57 |
| T20BD /0.5% wt/wt Graphene | 2073.1 ± 14.90 |
| T20BD /1% wt/wt Graphene | 2233.8 ± 54.43 |
| T20BD /4% wt/wt Graphene | 2274.1 ± 21.30 |

Young's Modulus increases from 2087 MPa for the unfilled resin to 2274 MPa for the filled resin (4% wt/wt graphene) giving an increase in percentage approximately equal to 9%.

### 3.3. Morphological analysis

Figs. 9-14 show FE-SEM micrographs of fracture surface of the samples tested in tensile mode. For each specimen, three types of micrographs are presented, one at a relatively low magnification and the others at higher magnification. The morphological investigation of the fracture surface of butt joints, highlights that the difference in the mechanical performance of the bonded joints in tensile tests, is closely correlated to the different distribution of the graphene in the epoxy matrix. The etched fracture surface of the bonding areas of B and C samples (see Figs. 9-10) evidences a failure in the adhesive part in the majority of the surface areas of the bonded parts. For both the samples, in fact, the mechanism of failure of bonded joint occurs into the layer of adhesive which remains on both adherent surfaces. The higher value of mechanical strength achieved for these sample with respect to sample A, is effectively due to the transfer of the external load to the adhesive which containing well dispersed graphene nanoplatelets that behave as the strongest part of the composite adhesive. Nevertheless, at higher nanofiller content (i.e. 4 wt/wt % ) (see sample D - Fig. 11), nanofiller aggregates of several microns determine strong heterogeneity in the morphological

feature of the resin. This occurrence is most likely responsible for the reduced value in the improvement of the tensile strength of joint with respect to the expected value.

The distribution of the graphene platelets in the epoxy matrix plays a crucial role in the adhesion. In fact, the tensile strength increases with the filler concentration, until, at higher concentration, the formation of aggregates causes discontinuity in the stress transfer inside the sample with a consequent decrease in the mechanical performance of the joint.

In the case of joints composed of filled adherents and filled epoxy paste (Figs. 12-14), it is possible to observe a failure in the adhesive part for sample E (see Fig. 12) which shows a good dispersion of graphene platelets in the adhesive paste covering both the surfaces of the adherents. For sample F of Fig. 13, it is possible to observe a good dispersion of graphene platelets in the adherents and adhesive past; due to the fact that the failure involves a large part of adherent material, as already described in the previous section, the failure in the adherents could be an almost certain signal of good adhesion.

For sample G (see Fig. 14), it is possible to observe clean parts of adherents indicative of adhesive failure in some regions (see the part of adherents surfaces) at the interphase between adhesive and adherents (see the region indicated as “part of adherents surfaces”). The lower value in the tensile strength with respect to other joints of the same series could be due to regions where the nanofiller aggregates cause a more easy debonding between some zones of adhesive and adherents.

The improvement of mechanical properties achieved with graphene platelets in the adhesive and adherents could be due to the intermolecular interactions, such as intermolecular hydrogen bonding between the hydroxyl or carboxylic groups of graphene platelets and cross-linked epoxy resins. This hypothesis seems to be confirmed by the additional benefit on the tensile strength of the joints filled with graphene platelets.

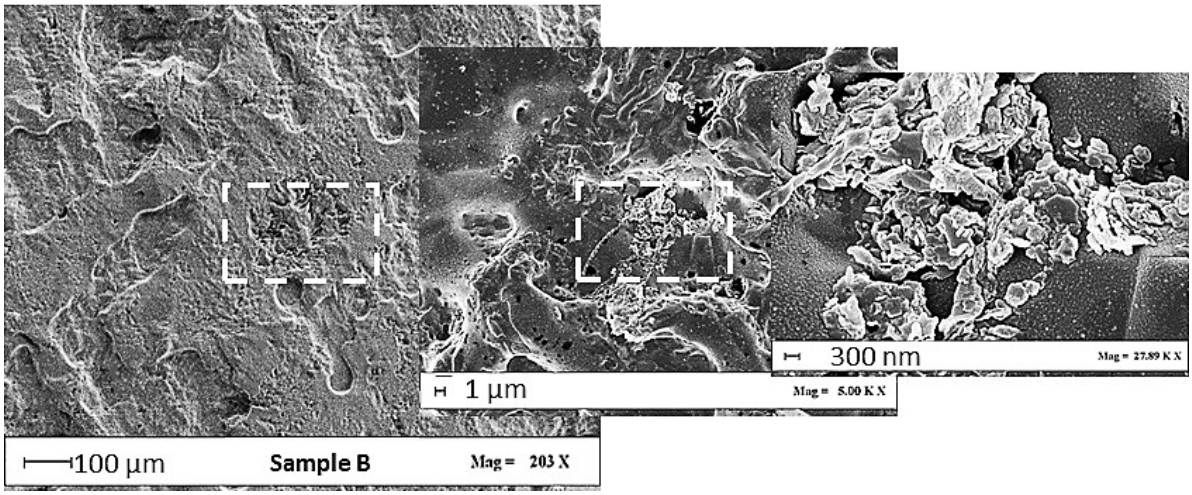


**Fig. 9** FESEM micrographs of fracture surfaces of the bonding areas of sample B. Failure in tensile test and detail of magnifications of neighbor region.

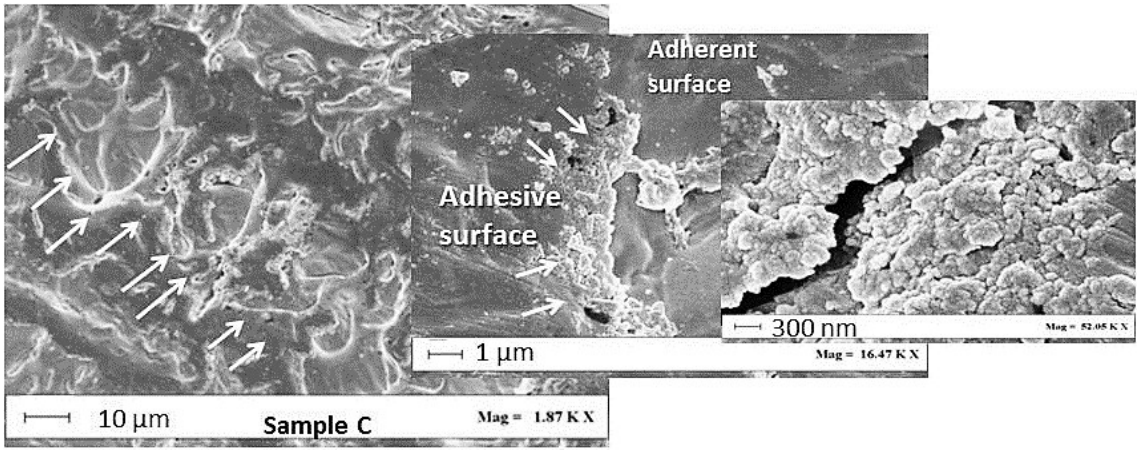


**Fig. 10** FESEM micrograph of fracture surfaces of the bonding areas-samples C. Failure in tensile test and detail of magnifications of neighbor region.

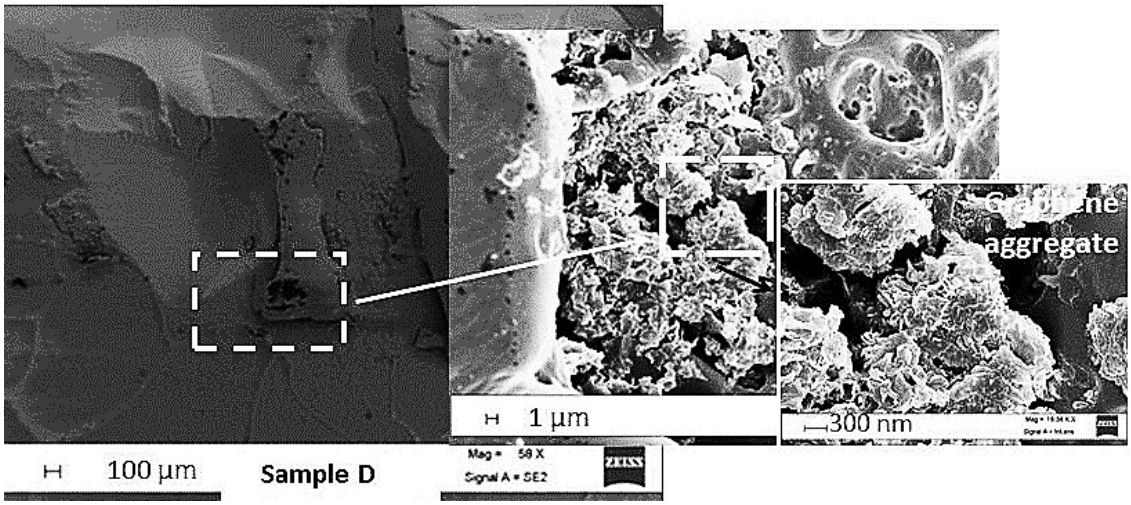


**Fig. 11** FESEM micrograph of fracture surfaces of the bonding areas-samples D. Failure in tensile test and detail of magnifications of neighbor region.

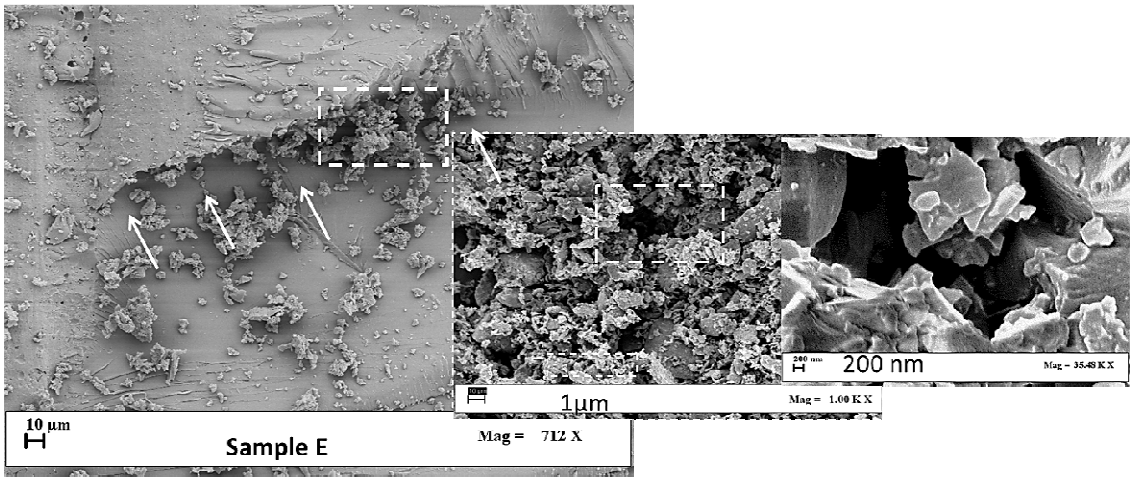


**Fig. 12** FESEM micrograph of fracture surfaces of the bonding areas-samples E. Failure in tensile test and detail of magnifications of neighbor region.

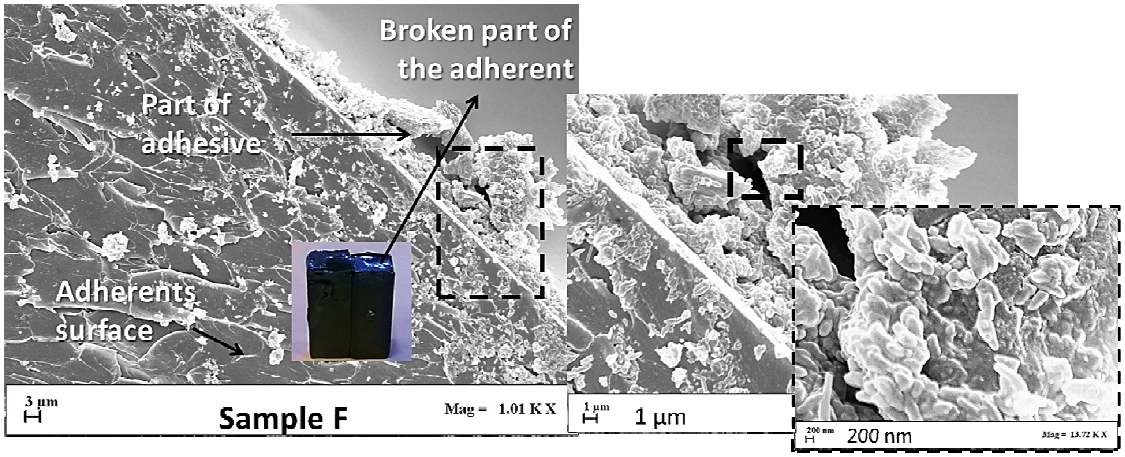


**Fig. 13** FESEM micrograph of fracture surfaces of the bonding areas-samples F. Failure in tensile test and detail of magnifications of neighbor region.

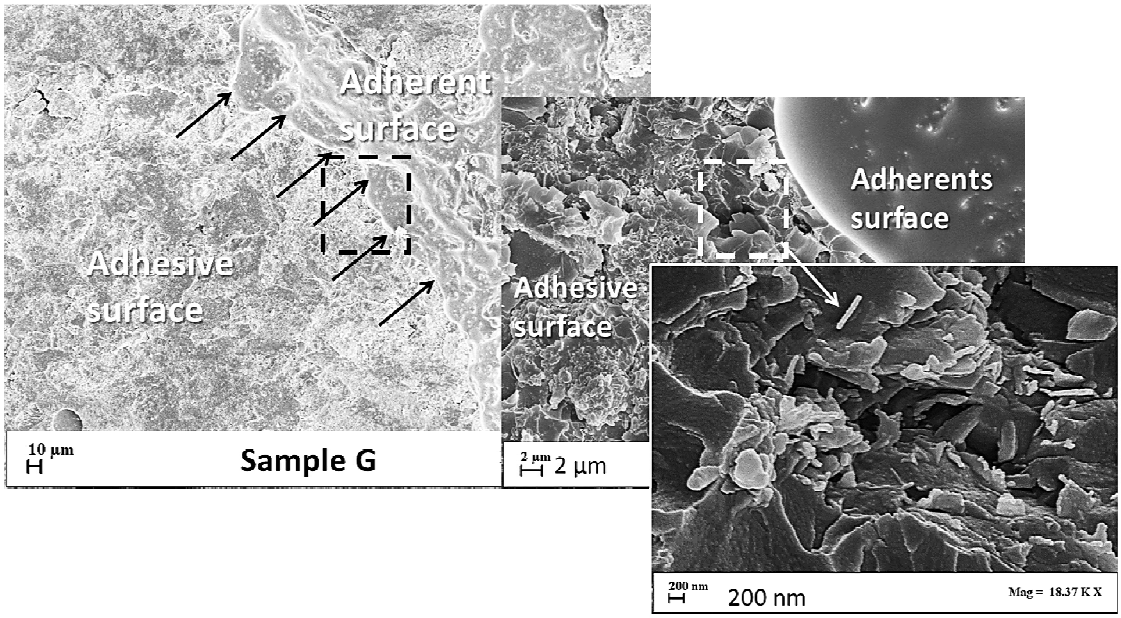


**Fig. 14** FESEM micrograph of fracture surfaces of the bonding areas-samples G. Failure in tensile test and detail of magnifications of neighbor region.

## 4. CONCLUSIONS

Graphene and multilayer graphene have been prepared by liquid phase exfoliation in N-methylpyrrolidone (NMP). The sonication concentration solution, time and ultrasound power have permitted to obtain a one step massive very pure production of thin platelets: the exfoliated graphite was 30 wt% of the original graphite (TG evaluation) and the monolayer yield was about 1.8 wt.%.

The reinforcement effect due to graphene platelets has proven to be very effective in improving the attractive interaction between adhesive and adherent surface. In fact, the addition of an appropriate amount of graphene platelets into an epoxy adhesive formulation designed for structural application caused a significant improvement in the mechanical performance of the joints. Amount equal or higher than 4%wt/wt have shown to be deleterious for the adhesive properties. The adverse effect is more probably due to aggregations and then poor dispersion of the nanofiller into the adhesive paste. A further improvement in the mechanical performance of the joints is achieved by adding graphene platelets also in the adherents. This beneficial effect could be due to the cumulative joined effects of intermolecular interactions, such as intermolecular hydrogen bonding between the hydroxyl or carboxylic groups of graphene platelets and OH groups of cross-linked epoxy resins. The application of this strategy to increase attractive forces at the interphase between adhesive and adherents has the potential to open new scenarios and opportunities in the design of innovative joints allowing to expand the use of adhesive bonding of structural parts, increasing the competitiveness of the industries in terms of performance and cost. It is worth noting that the inclusion of conductive nanofiller in adhesives for composite structures has also the prospective to obtain multifunctional adhesives, able to integrate simultaneously the structural mechanical performance and the required electrical conductivity. The appropriate selection and modification of the polymer matrix composition, the nanofiller type and the control of the interactions at the interphase could allow to obtain tailored multifunctional properties of the resulting adhesive, which could otherwise not be achieved by conventional materials or composites.

**ACKNOWLEDGEMENTS**

This research has received funding from the European Union's Seventh Framework Programme for research, technological development and demonstration under grant agreement n$^{o}$ 313978.

## REFERENCES

[1] L. Guadagno, M. Raimondo, K. Lafdi, A. Fierro, S. Rosolia and M. R. Nobile, Influence of nanofiller morphology on the viscoelastic properties of CNF/epoxy resins, *AIP Conf. Proc.*, 2014, **1599,** 386-389.

[2] L. Guadagno, M. Raimondo, U. Vietri, L. Vertuccio, G. Barra, B. De Vivo, P. Lamberti, G Spinelli, V. Tucci, R. Volponi, G. Cosentino and F. De Nicola, Effective Formulation and Processing of nanofilled Carbon Fiber Reinforced Composites, *RSC Adv*., 2015, **5**, 6033-6042.

[3] L. Guadagno, M. Raimondo, V. Vittoria, L. Vertuccio, C. Naddeo, P. Lamberti and V. Tucci, *Italian Patent* "Resina epossidica con basso tenore di umidità" No. TO2013A000926 (15 November 2013).

[4] L. Guadagno, M. Raimondo, V. Vittoria, L. Vertuccio, C. Naddeo, S. Russo, B. De Vivo, P. Lamberti, G. Spinelli and V. Tucci, Development of epoxy mixtures for application in aeronautics and aerospace, *RSC Adv*., 2014, **4**, 15474-15488.

[5] K. T. Hsiao, J. Alms and S. G. Advani, Use of epoxy/multiwalled carbon nanotubes as adhesives to join graphite fiber reinforced polymer composites, *Nanotechnology*, 2003, **14**, 791-793.

[6] S. Yu, M. N. Tong and G. Critchlow, Wedge test of carbon-nanotube-reinforced epoxy adhesive joints, *J. Appl. Polym. Sci.*, 2009, **111**, 2957-2962.

[7] S. A. Meguid and Y. Sun, On the tensile and shear strength of nano-reinforced composite interfaces, *Mater. Des*., 2004, **25**, 289-296.

[8] U. Vietri, L. Guadagno, M. Raimondo, L. Vertuccio and K. Lafdi, Nanofilled epoxy adhesive for structural aeronautic materials, *Compos Part B-Eng*., 2014, **61**, 73-83.

[9] A. S. Neto, D. T. L. Da Cruz and A. F. Ávila , Nano-modified adhesive by graphene: The single lap-joint case, *Mater. Res*., 2013, **16**, 592-596.

[10] F. H. Gojny, M. H. G. Wichmann, B. Fiedler, W. Bauhofer and K. Schulte, Influence of nano-modification on the mechanical and electrical properties of conventional fibre-reinforced composites, *Compos. Part A-Appl. Sci. Manuf.*, 2005, **36**, 1525-1535.

[11] T. Wang, C. H. Lei, A. B. Dalton, C. Creton, Y. Lin, K. A. S. Fernando, Y. P. Sun, M. Manea, J. M. Asua and J. L. Keddie Waterbone, Nanocomposite Pressure-Sensitive Adhesives with High Tack Energy, Optical Transparency, and Electrical Conductivity, *Adv. Mater.*, 2006, **18**, 2730-2734.

[12] C. W. Nan, Y. Shen and J. Ma, Physical Properties of Composites Near Percolation, *Annu. Rev. Mater. Res.*, 2010, **40**, 131-151.

[13] L. Guadagno, B. De Vivo, A. Di Bartolomeo, P. Lamberti, A. Sorrentino, V. Tucci, L. Vertuccio and V. Vittoria, Effect of functionalization on the thermo-mechanical and electrical behavior of multi-wall carbon nano tube/epoxy composites, *Carbon*, 2011, **49**, 1919-1930.

[14] B. De Vivo, L. Guadagno, P. Lamberti, M. Raimondo, G. Spinelli, V. Tucci, L. Vertuccio and V. Vittoria, Electrical properties of multi-walled carbon nano tube/tetrafunctional epoxy-amine composites, *AIP Conf. Proc.*, 2012, **1459**, 199-201.

[15] L. Guadagno, M. Raimondo, V. Vittoria, L. Vertuccio, K. Lafdi, B. De Vivo, P. Lamberti, G. Spinelli and V. Tucci, The role of carbon nanofiber defects on the electrical and mechanical properties of CNF-based resins, *Nanotechnology*, 2013, **24**, 305704 (10pp).

[16] S. G. Prolongo, M. R. Gude and A. Ureña, Nanoreinforced Adhesives In *Nanotechnology and Nanomaterials "Nanofibers"* book edited by Ashok Kumar Publisher *InTech* Chapter 3, 2010, pp 39-68 ISBN 978-953-7619-86-2.

[17] A. K. Geim and K. S. Novoselov, The rise of graphene, *Nat. Mater.*, 2007, **6**, 183-191.

[18] T. J. Echtermeyer, M. C. Lemme, M. Baus, B. N. Szafranek, A. K. Geim and H. Kurz, Nonvolatile switching in graphene field-effect devices, *IEEE Electron Dev. Lett.*, 2008, **29**, 952-954.

[19] G. Eda, G. Fanchini and M. Chhowalla, Large-area ultrathin films of reduced graphene oxide as a transparent and flexible electronic material, *Nat. Nanotechnol.*, 2008, **3**, 270-274.

[20] K. S. Kim, Y. Zhao, H. Jang, S. Y. Lee, J. M. Kim, K. S. Kim, J. H. Ahn, P. Kim, J. Y. Choi and B. H. Hong, Large-scale pattern growth of graphene films for stretchable transparent electrodes, Nature, 2009, **457**, 706-710.

[21] P. Blake, P. D. Brimicombe, R. R. Nair, T. J. Booth, D. Jiang, F. Schedin, L. A. Ponomarenko, S. V. Morozov, H. F. Gleeson, E. W. Hill, A. K. Geim and K. S. Novoselov, Graphene-based liquid crystal device, *Nano Lett.*, 2008, **8**, 1704-1708.

[22] M. D. Stoller, S. Park, Y. Zhu, J. An and R. S. Ruoff, Graphene-Based Ultracapacitors, *Nano Lett.*, 2008, **8,** 3498-3502.

[23] D. A. Dikin, S. Stankovich, E. J. Zimney, R. D. Piner, G. H. B. Dommett, G. Evmenenko, S. T. Nguyen and R. S. Ruoff, Preparation and characterization of graphene oxide paper, *Nature*, 2007, **448**, 457-460.

[24] J. S. Bunch, S. S. Verbridge, J. S. Alden, A. M. van der Zande, J. M. Parpia, H. G. Craighead, P. L. McEuen, *Nano Letters*, 2008, **8**, 2458-2462.

[25] N. Yan, G. Buonocore, M. Lavorgna, S. Kaciulis, S. K. Balijepalli, Y. Zhan, H. Xia and L. Ambrosio, The role of reduced graphene oxide on chemical, mechanical and barrier properties of natural rubber composites, *Composites Science and Technology*, 2014, **102**, 74-81.

[26] G. Scherillo, M. Lavorgna, G. G. Buonocore, Y. H. Zhan, H. S. Xia, G. Mensitieri and L. Ambrosio, Tailoring assembly of reduced graphene oxide nanosheets to control gas barrier properties of natural rubber nanocomposites, *ACS Applied Materials & Interfaces*, 2014, **6**, 2230-2234.

[27] S. Stankovich, D. A. Dikin, R. D. Piner, K. A. Kohlhaas, A. Kleinhammes, Y. Jia, Y. Wu, S. T. Nguyen and R. S. Ruoff, Synthesis of graphene-based nanosheets via chemical reduction of exfoliated graphite oxide, *Carbon*, 2007, **45**, 1558-1565.

[28] Y. Hernandez, V. Nicolosi, M. Lotya, F. M. Blighe, Z. Sun, S. De, I. T. McGovern, B. Holland, M. Byrne, Y. K. Gun'ko, J. J. Boland, P. Niraj, G. Duesberg, S. Krishnamurthy, R. Goodhue, J. Hutchison, V. Scardaci, A. C. Ferrari and J. N. Coleman, High-yield production of graphene by liquid-phase exfoliation of graphite, *Nature Nanotechnology*, 2008, **3**, 563-568.

[29] A. Reina, X. Jia, J. Ho, D. Nezich, H. Son, V. Bulovic, M. S. Dresselhaus, J. Kong, Large Area, Few-Layer Graphene Films on Arbitrary Substrates by Chemical Vapor Deposition, *Nano Lett.*, 2009, **9**, 30-35.

[30] Y. Lee, S. Bae, H. Jang, S. Jang, S. E. Zhu, S. H. Sim, Y. I. Song, B. H. Hong and J. H. Ahn, Wafer-Scale Synthesis and Transfer of Graphene Fims, *Nano Lett.*, 2010, **10,** 490-493.

[31] M. Sarno, C. Cirillo, R. Piscitelli and P. Ciambelli, A study of the key parameters, including the crucial role of $H_2$ for uniform graphene growth on Ni foil, *J. Mol. Catal. A: Chem.*, 2013, **366**, 303-314.

[32] M. Sarno, C. Cirillo and P. Ciambelli, Selective graphene covering of monodispersed magnetic nanoparticles, *Chem. Eng. J.*, 2014, **246**, 27-38.

[33] M. Funaro, M. Sarno, P. Ciambelli, C. Altavilla and A. Proto, Real time radiation dosimeters based on vertically aligned multiwall carbon nanotubes and graphene, *Nanotechnology*, 2013, **24,** 075704 (7 pp).

[34] Z. Chen, W. Ren, B. Liu, L. Gao, S. Pei, Z. S. Wu, J. Zhao and H. M. Cheng, Bulk-growth of mono-to few-layer graphene on nickel particles by chemical vapor deposition from methane, *Carbon*, 2010, **48**, 3543-3550.

[35] M. Sarno, A. Senatore, C. Cirillo, V. Petrone and P. Ciambelli, Oil lubrificant tribological behaviour improvement through dispersion of few layer graphene oxide, *J.Nanosci. Nanotechnol.*, 2014, **14**, 4960-4968.

[36] J. C. Meyer, A. K. Geim, M. I. Katsnelson, K. S. Novoselov, T. J. Booth and S. Roth, The structure of suspended graphene sheets, *Nature*, 2007, **446**, 60-63.

[37] S. Y. Bae, I. Y. Jeon, J. Yang, N. Park, H. Suk Shin, S Park, R. S. Ruoff, L. Dai and J. B. Baek, Large-Area Graphene Films by Simple Solution Casting of Edge-Selectively Functionalized Graphite, *ACS Nano*, 2011, **5**, 4974-4980.

[38] C. Casiraghi, A. C. Ferrari and J. Robertson, Raman Spectroscopy of hydrogenated amorphous carbons, *Phys. Rev. B*, 2005, **72**, 085401 (14 pp).

[39] A. C. Ferrari, S. E. Rodil and J. Robertson, Interpretation of infrared and Raman spectra of amorphous carbon nitrides, *Phys. Rev. B*, 2003, **67,** 155306 (20 pp).

[40] L. M. Malard, M. A. Pimenta, G. Dresselhaus and M. S. Dresselhaus, Raman Spectroscopy in graphene, *Phys. Rep.*, 2009, **473**, 51-87.

[41] A. C. Ferrari, Raman spectroscopy of graphene and graphite: Disorder, electron-phonon coupling, doping and nonadiabatic effects, *Solid State Communication*, 2007, **143**, 47-57.